NANO LETTERS
Cite This: Nano Lett. 2017, 17, 6847-6854
Letter
pubs.acs.org/NanoLett

Diversifying Nanoparticle Assemblies in Supramolecule Nanocomposites Via Cylindrical Confinement

Peter Bai,[†] Sui Yang,[‡] Wei Bao,[†,∥] Joseph Kao,[†] Kari Thorkelsson,[†] Miquel Salmeron,[†,∥] Xiang Zhang,[‡,∥] and Ting Xu*[,†,⊥,∥]

[†]Department of Materials Science and Engineering, [‡]Department of Mechanical Engineering, [⊥]Department of Chemistry, University of California, Berkeley, California 94720, United States

[∥]Materials Sciences Division, Lawrence Berkeley National Laboratory, Berkeley, California 94720, United States

Supporting Information

ABSTRACT: Many macroscopic properties such as collective chiral responses enhanced by coupled plasmonic nanoparticles require complex nanostructures. However, a key challenge is to directly assemble nanosized building blocks into functional entities with designed morphologies. For example, the DNA templated nanoparticle assembly has low scalability and requires aqueous conditions, while other approaches such as controlled drying and polymer templating access only simple 1-D, 2-D, and 3-D structures with limited assembly patterns. Here, we demonstrate a new self-assembly strategy that expands the diversity of 3-D nanoparticle assemblies. By subjecting supramolecular nanocomposites to cylindrical confinement, a range of new nanoparticle assemblies such as stacked rings and single and double helices can be readily obtained with a precisely defined morphology. Circular dichroism dark field scattering measurements on the single nanowire with Au helical ribbon-like assembly show chiral plasmonic response several orders of magnitude higher than that of natural chiral materials. The phase behavior of supramolecular nanocomposite under geometric constraints is quite different from that of block copolymer. It depends on the complex interplay among nanoparticle packing and phase behavior of parent block copolymers under confinement and can be governed by nanoparticle diffusion.

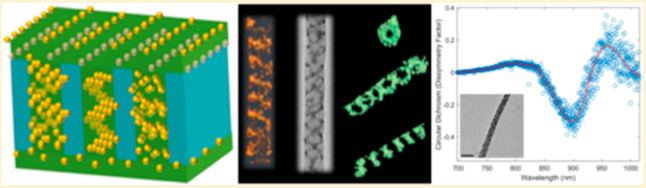

KEYWORDS: *Helical nanoparticle ribbon, supramolecular nanocomposite, cylindrical confinement, infrared chirality*

The nanoparticle (NP), the so-called artificial atom, has demonstrated unique properties not accessible in bulk material. Directed NP assembly enables one to access new properties arising from the interparticle couplings.[1−10] Generating NP-containing building blocks is also crucial to constructing mesoscale materials.[11] However, there are only limited success cases where curved 3-D NP assemblies have been produced. Controlled drying and pattern-guided assembly are limited to NP assemblies on a surface.[12−14] Nanocomposites, that is, polymer/NP blends, can generate 1-, 2-, and 3-D ordered NP arrays but only exhibit rather simple patterns.[15,16] Experimentally, we still cannot realize NP assemblies beyond typical block copolymer (BCP) morphologies. DNA-guided assembly is versatile, but limited to aqueous media and types of NPs compatible with DNA surface modification.

Geometric confinement is effective in generating complex nanostructures in BCPs as shown experimentally and theoretically by modulating entropy associated with BCP incommensurability.[17−19] However, one cannot directly extrapolate similar morphological control in the blends of BCP and NP due to several reasons. The incorporation of NP into BCP microdomains requires favorable NP ligand/BCP interaction and can be limited by particle surface chemistry and BCP composition.[20] The presence of NP within BCP leads to changes in the polymer chain conformation. Previous studies have shown that the entropic conformational contribution affects NP spatial distribution and can lead to macrophase separation between NP and BCP.[15,21,22] In the geometric confined system, the confining dimension approaches the natural periodicity of the BCP/NP blend. The effect from the entropic contribution is expected to be energetically comparable to the incommensurability effect for BCP alone. In fact, there is no report that experimentally realized complex NP assemblies in BCP/NP blends. In situ NP synthesis within BCP framework has been very successful in realizing inorganic nanostructures.[23−26] Nanocomposites based on presynthesized NPs have many advantages such as controlling the NP size, manipulating inter-NP coupling, and/or using mixtures of NPs to access synergistic coupling effects. Supramolecules are constructed by noncovalently attaching small molecules to BCP side chains.[27] The small molecule mediates the NP/polymer interaction and changes polymer chain architecture and rigidity, leading to ordered NP assemblies without surface modification of NP for a range of NP size, shape, and chemical composition.[28] While these features open opportunities to use geometric constraints to access complex assemblies of NPs, it

Received: July 23, 2017
Revised: September 22, 2017
Published: October 2, 2017

DOI: 10.1021/acs.nanolett.7b03131
Nano Lett. 2017, 17, 6847−6854

Scheme 1. Fabrication of Supramolecular Nanocomposite Nanowires

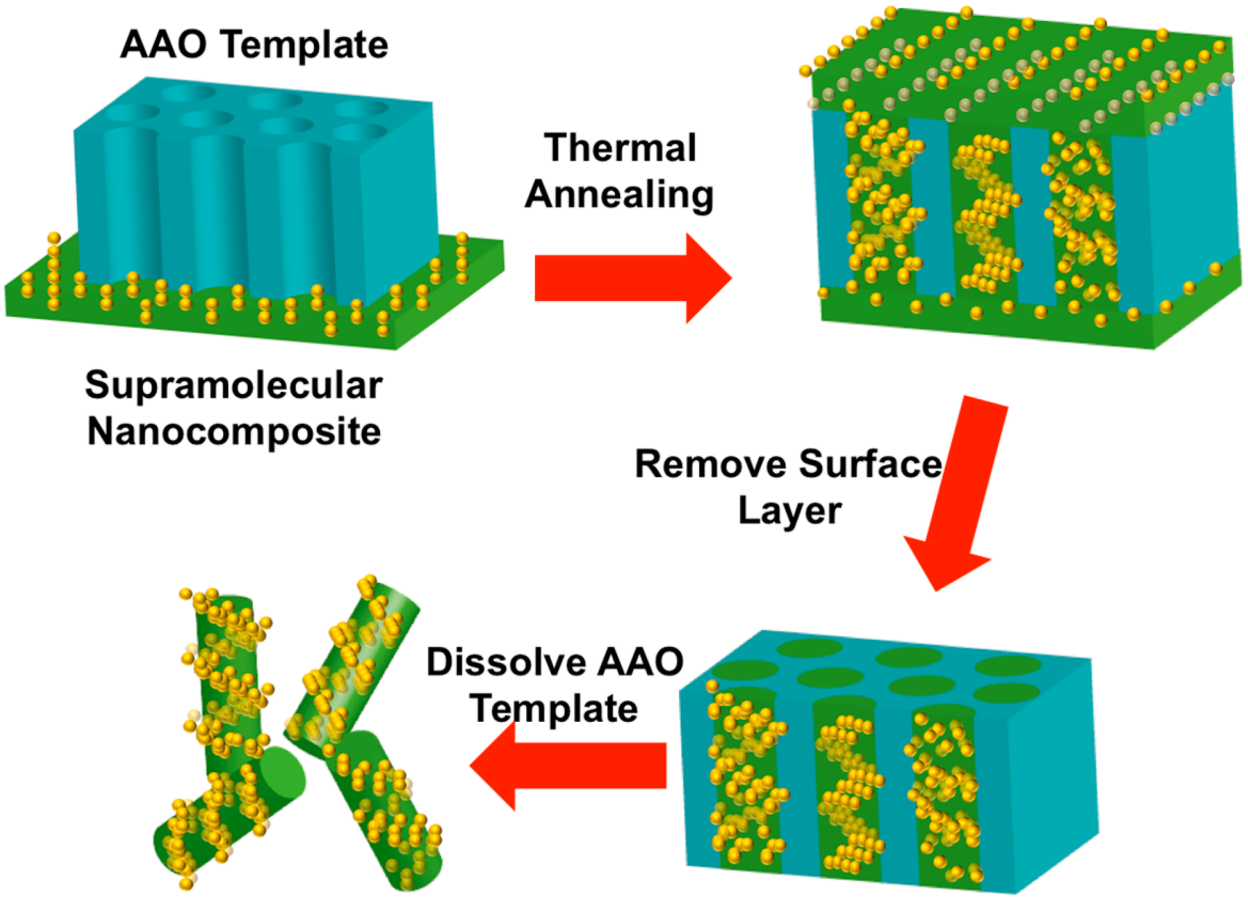

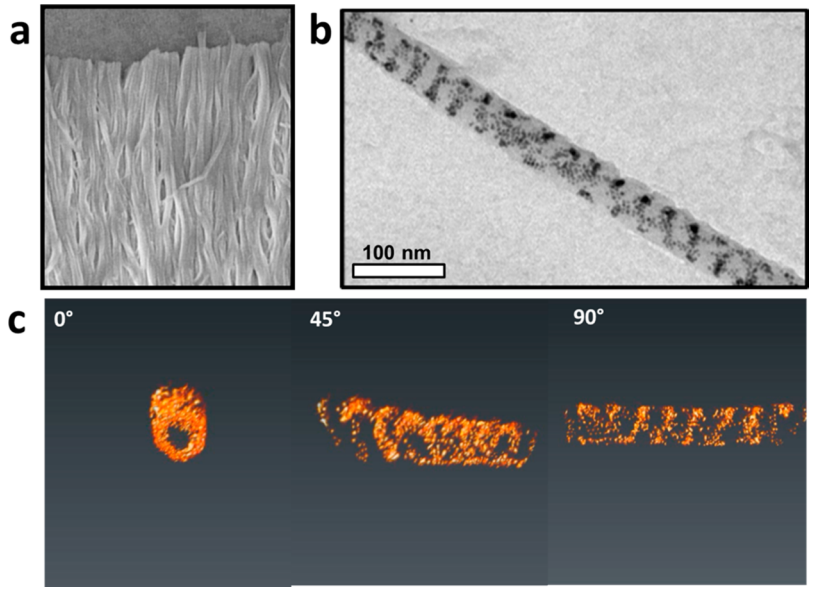

Figure 1. Structural characterization of NP helical assembly. (a) SEM image of high density arrays of nanowires comprised of PS-*b*-P4VP(PDP)$_{1.7}$ and 9 vol % 4 nm Au NP. (b) TEM image of a single nanowire shows helical nanostructure. (c) 3-D TEM tomography reconstruction of the nanowire oriented at 0°, 45°, and 90° relative to its long axis confirms the helical nanostructure.

also adds significant complexity since small molecules can be redistributed during the assembly process.

Here we show that, upon imposing cylindrical confinement, the supramolecular nanocomposite can form a range of complex 3-D NP assemblies. In particular, a single nanocomposite nanowire containing Au NP helical ribbon-like assembly exhibits near-infrared (NIR) chirality with a strong *g*-factor value comparable to the highest reported to date. Equally importantly, the phase behavior of supramolecular nanocomposite under cylindrical confinement is not in agreement

DOI: 10.1021/acs.nanolett.7b03131
Nano Lett. 2017, 17, 6847−6854

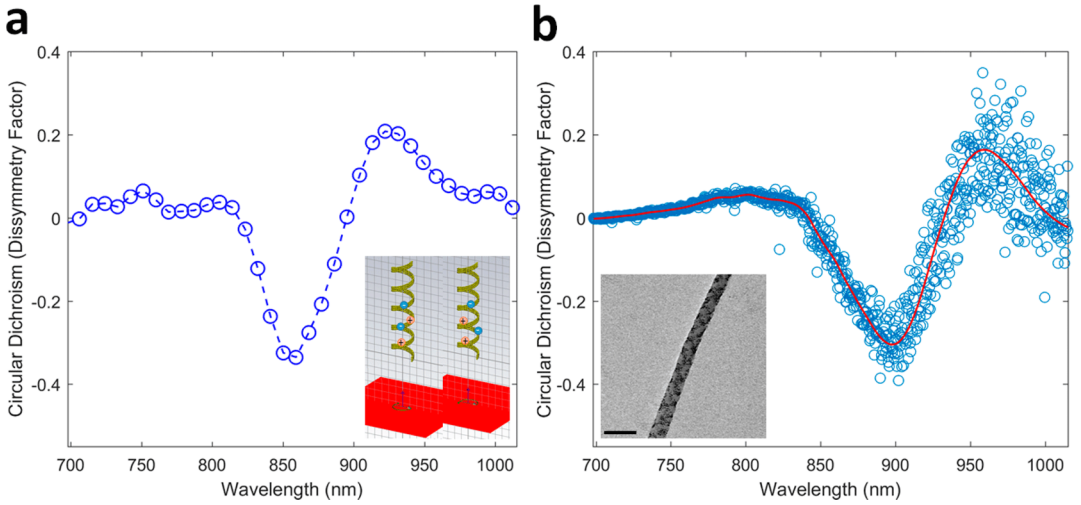

Figure 2. Chiral plasmonic response of a single helical Au NP assembly. (a) Simulated CD spectrum with the inset showing the induced charge distribution in right-handed helices of Au NP within different circularly polarized electromagnetic field excitations. (b) Single molecule dark field scattering measurement of the NP helical assembly (inset), demonstrating CD in the NIR regime. The TEM scale bar is 100 nm.

with any of previous theoretical predictions for BCP/NP blends. Experimentally, the NP assemblies within a composite nanowire are independent of supramolecular composition/morphology. Rather, they are mainly governed by the NP loading and parent BCP composition and subject to degeneracy. The resultant complex 3-D NP assemblies may reflect interplay between NP packing under confinement and phase behavior of parent BCP and can be governed by nanoparticle diffusion, thus opening a new platform to manipulate NP assembly and inter-NP coupling to obtain new properties.

Results and Discussion. The supramolecule, PS(19K)-*b*-P4VP(5.2K)$(PDP)_{1.7}$, is composed of polystyrene(19 kDa)-*block*-poly(4-vinylpyridine)(5.2 kDa) (PS-*b*-P4VP) with 3-*n*-pentadecylphenol (PDP) hydrogen bonded to the 4VP units at a 1.7 PDP:4VP ratio. PS-*b*-P4VP$(PDP)_{1.7}$ mixed with 9 vol % 4 nm dodecanethiol-capped Au NPs is drop-cast onto an anodic aluminum oxide (AAO) membrane and thermally annealed at 110 °C (Scheme 1). The 35 nm AAO membrane was used to impose cylindrical confinement. The resulting composite nanowires are ∼35 nm in width spanning tens of micrometers (Figure 1a). In bulk, PS(19K)-*b*-P4VP(5.2K)$(PDP)_{1.7}$ form hexagonally packed cylindrical morphology and, upon incorporation of 4 nm NPs, form hexagonally packed 1-D NP chains with a lateral periodicity of 30 nm.[28] Once confined in a 35 nm nanowire, the in-plane TEM image shows that, in single nanocomposite nanowire, the 4 nm Au NPs form a single helix (several microns in length), ∼30 nm in diameter with a pitch ranging from 20 to 50 nm (Figure 1b). The NP helical structure is confirmed via 3-D TEM tomography. Figure 1c shows the tomography reconstruction of the NP helix oriented at 0°, 45°, and 90° with respect to its axis (tomography reconstruction videos available in Supporting Information). Different from the NP helical structures prepared via DNA,[3,7,29] peptide,[30,31] or small molecules[32] where the helices are composed of one NP string, the NP helical structure within the nanowires contains 3−4 particles along the direction perpendicular to the helix axis. However, the NP organization is not continuous along the helix axis; thus, the observed morphology is more accurately depicted as a NP helical ribbon-like assembly. Such a structure provides a higher degree of freedom to tailor interparticle interactions along different directions to modulate properties of nanoparticle clusters.

The geometry of the NP helical assembly should give rise to intriguing chiro-optical behavior. The frequency of the circular dichroism (CD) signal is related to the polarizability of NP chain and can be described by

$$\alpha = AV\frac{\varepsilon - \varepsilon_b}{\varepsilon_b + L(\varepsilon - \varepsilon_b)} \quad (1)$$

where V is the volume of metal in the system, ε and ε_b are the permittivities of the metal and the background, respectively, A is a strength factor, and L is the geometry-dependent depolarization factor.[33] In most of the previous studies, NP helices showed a chiral response in the wavelength range, ∼500−600 nm and can be shifted to slightly above 600 nm by using larger NPs, nanorods, or different chemical compositions.[3,29,31,34] With the formation of helical assembly, the volume of metal is much higher that that in a single NP helix. Equally important is that the Au NPs are placed in close proximity for inter-NP coupling in both directions parallel and perpendicular to the helix axis. Together, these features may lead to strong chiral optical responses in the near-infrared (NIR) regime.[35]

We developed a dark field single-particle CD spectroscopy technique (SI 3) to measure the optical property of a single helical NP assembly due to the lack of preferential handedness in confined assembly. With an oblique circular polarized light excitation, the scattered light from a single nanowire is selectively collected by placing a pinhole at a re-imaged focal plane. The chiroptical property can be evaluated by measuring the Kuhn dissymmetry factor (g-factor), defined as the CD signal normalized by its corresponding scattering as $2(S_L - S_R)/(S_L + S_R)$.[36,37] Figure 2 shows the calculated (Figure 2a) and measured CD spectra (Figure 2b) that are in reasonably good agreement. The small discrepancy in wavelength can be attributed to the NP size distribution and nonuniform spacing between NPs (SI discussion 2). The measured spectrum in Figure 2b shows a clear vertically mirrored, bi-signated dip-peak in the range of 800−1000 nm. This arises from the collective cross coupling of plasmonic dipole of Au NPs and phase lag along the propagation direction of the excitation light beam and

DOI: 10.1021/acs.nanolett.7b03131
Nano Lett. 2017, 17, 6847−6854

conforms well to the calculated spectrum (Figure 2a). This bisignated dip-peak CD response is in contrast to the regular Cotton effect observed in chiral molecules and can be attributed to the dipole−dipole interactions between cross coupled NPs and the substantial scattering cross-section of micron-sized helical nanoribbon.[3,38−40] Notably, the *g*-factor values are 0.31 at $\lambda \sim 895$ nm and 0.17 at $\lambda \sim 960$ nm. The measured *g*-factor of Au NP ribbon is orders of magnitude higher than typical chiral materials and is comparable to the highest value ($g \sim 0.4$) reported to date.[37,41] The typical *g*-factor value is in the range of $\sim 10^{-7}$ to $\sim 10^{-5}$ for natural chiral optical materials,[42] and in the range of $\sim 10^{-3}$ to $\sim 10^{-2}$ for most of DNA-guided chiral assemblies using spherical NPs.[43,44] The strong plasmonic chirality realized in the NIR range (Figure 2) provides opportunities to fabricate NP-based devices for biomolecular enantiomer detection,[45] vibrational CD sensing,[46] and chiral metamaterials.[47]

Although it remains a challenge to globally control the handness of the NP helical ribbon-like assembly, the NP helix results validate the experimental feasibility to access a complex 3-D NP assembly with new properties by a geometrically confining supramolecular nanocomposite. The supramolecular approach has been applied successfully to assemble NPs with different sizes, shapes, and core chemistries and offers opportunities to obtain complex NP assemblies unattainable otherwise. To fully realize their potential, we need to identify the key factors governing the phase behavior of the supramolecular system under cylindrical confinement. Previous studies show that the morphologies of BCPs or BCP-based supramolecule determine the spatial arrangement of NPs in bulk.[16,22,28] The addition of small molecule and NPs leads to many complications in the overall energy landscape. We first study the effects of cylindrical confinement for the supramolecule alone. Figure 3a shows the 35 nm nanowire composed of PS(19K)-*b*-P4VP(5.2K)$(PDP)_{1.7}$ alone, where the P4VP(PDP) microdomains are selectively stained by exposing to iodine vapor. In each nanowire, there are two rows of P4VP(PDP) spheres/ellisoids embedded in the PS matrix. The majority component is PS. This is drastically different from its morphology in bulk with the PS cylinder embedded in the P4VP(PDP) matrix. The cylindrical confinement not only leads to a cylinder-to-sphere morphological transition but also changes the local composition of the supramolecule within the nanowire. In comparison to pure BCPs under similar cylindrical confinement,[48] the morphological change achieved here is more dramatic and indicates the strong susceptibility of supramolecular systems to confinement-induced morphological changes.

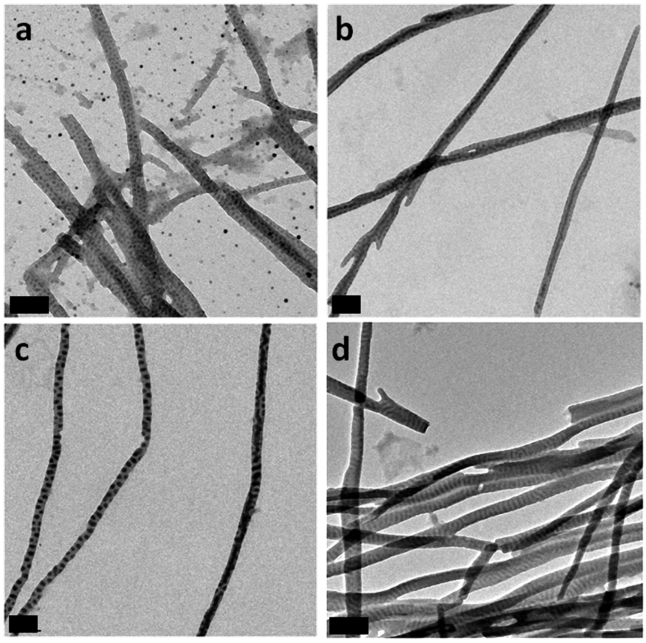

Figure 3. Effect of f_{P4VP} on cylindrically confined supramolecules. TEM images of cylindrically confined supramolecules (a) I, (b) II, (c) III, and (d) IV stained with I_2 vapor. Scale bars are 200 nm for all images.

Further studies show that the morphology of supramolecule in a nanowire is mainly governed by the parent BCP used to construct the supramolecule. However, no NP assembly can be obtained in blends of PS-*b*-P4VP/NP under similar conditions. Varying PDP:4VP stoichiometry from 0.7 to 3 changes the P4VP(PDP) volume fraction from 0.22 to 0.74. However, a similar morphology was observed for all PDP:4VP ratios studied (SI 4). Supramolecules were also constructed using PS-*b*-P4VP BCPs with different P4VP volume fractions (f_{P4VP}). The PDP:4VP ratio was varied to achieve the same P4VP(PDP) comb block volume fraction (f_{comb}) (Table 1). As shown in Figure 3b−d, the resulting nanowires have morphologies similar to that of the parent BCP rather than that of supramolecule.

Table 1. Supramolecules Used To Investigate the Effect of f_{P4VP} on the Resulting Supramolecule Morphology under Cylindrical Confinement

sample no.	BCP	PDP:4VP ratio	f_{P4VP}	f_{comb}
I	PS(19 kDa)-*b*-P4VP(5.2 kDa)	1.7	0.22	0.62
II	PS(32.1 kDa)-*b*-P4VP(13.2 kDa)	1.3	0.29	0.62
III	PS(20 kDa)-*b*-P4VP(19 kDa)	0.8	0.49	0.62
IV	PS(11.8 kDa)-*b*-P4VP(15 kDa)	0.7	0.56	0.62

The PDP small molecules play an important role in the phase behavior of the supramolecule/NP system under 2-D confinement. The incorporation of NPs into supramolecular system relies on favorable intermolecular interactions between the NP ligands and PDP. The formation of NP helical assembly confirms the presence of PDP within the P4VP-rich microdomain. This PDP redistribution has been well-documented in bulk PS-*b*-P4VP(PDP) systems under thermal annealing using in situ FTIR and small-angle scattering techniques.[27,49] During thermal annealing, the PDP can be detached from the P4VP(PDP) block due to the noncovalent nature of the 4VP-PDP hydrogen bond. When heated above 100−110 °C, the PDP becomes miscible in the PS microdomain. We also confirmed the redistribution of PDP between the PS and P4VP(PDP) microdomains during thermal annealing in the supramolecular nanocomposites.[28] In thin films of PS-*b*-P4VP(PDP) supramolecules, PDP molecules also redistribute to balance interfacial interaction and minimize deformation in BCP chain conformation.[50] In Figure 3d, the microdomain is oriented normal to the nanowire axis and both PS and P4VP(PDP) microdomains contact the AAO membrane. This suggests a neutral interfacial condition and is analoguous to that observed in the supramolecule thin films.[50] Thus, upon being

DOI: 10.1021/acs.nanolett.7b03131
Nano Lett. 2017, 17, 6847−6854

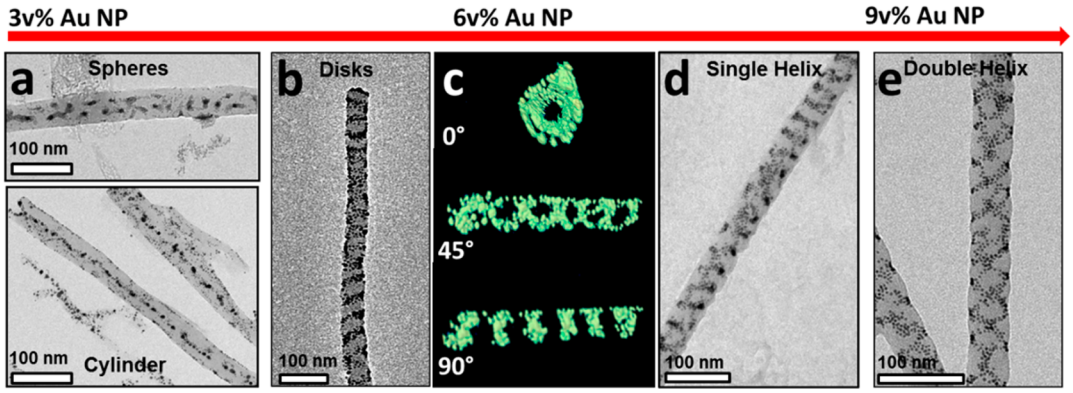

Figure 4. TEM of nanostructures in supramolecular nanocomposite nanowires. Different NP structures are predominant as a function of varying NP loading in the PS-*b*-P4VP(PDP)$_{1.7}$ supramolecule/Au NP blends under cylindrical confinement: (a) spherical NP clusters and 1-D NP arrays at 3 vol % NP loading; (b) TEM and (c) TEM tomography of stacked NP rings perpendicular to pore axis at 6 vol % NP loading; (d) single and (e) double helices observed along with single helices at 9 vol % NP loading.

confined in the AAO membrane, the free PDP molecules migrate to the cylindrical pore walls to modulate the polymer/substrate interfacial interaction. In cylindrical pores, this PDP migration mechanism would more strongly impact the self-assembly process due to the higher interfacial area to volume ratio in 2-D cylindrical confinement. Together all these observations may explain why the supramolecule morphology is quite insensitive to PDP loading, and the observed morphologies deviate from pure BCP systems under similar confinement conditions. Thus, the results suggest that the supramolecular system is not only effective in directing NP assembly under 2-D confinement but also can self-adjust PDP incorporation to mitigate incommensurability and minimizing energetic penalty associated with polymer chain conformation.

The incorporation of NPs affects polymer chain conformation and the spatial distribution of PDP. Varying NP loading will not only modulate these energetic contributions but also the number of NPs in each nanowire. Upon adding 3 nm NPs, different morphologies were observed. As shown in Figure 4a, at low NP loadings (3 vol %), Au NPs form double rows of spherical NP clusters (top) or single NP arrays oriented parallel to the axis of the nanowire (bottom). The NP morphology closely resembles that of the supramolecule nanowire. Although there is a significant difference in morphologies of supramolecule in bulk and in nanowire, the spatial distribution of NPs is primarily guided by the supramolecule. Upon increasing NP loading, however, the NP assembly deviates from that of supramolecule nanowire. A rich library of complex NP assemblies emerges. At 6 vol % NP loading, a NP "disk" morphology becomes predominant where NPs form "disks" that stack along the axis of the nanowire (Figure 4b). Figure 4c shows a snapshot of the 3-D TEM tomographic rendering of the perpendicular stacked disk morphology at 0° (top), 45° (middle), and 90° (bottom) to the AAO pore axis. The "disks" observed in the 2-D in-plane TEM images are revealed to be hollow rings with a thickness of ∼15 nm, ∼40 nm in pitch, and ∼35 nm in diameter, and the NPs reside at the surface of the nanowires (see SI for movie of TEM tomography reconstruction of stacked NP rings). Upon further increasing the NP loading to 9 vol %, nanowires with single or double helical ribbon morphology are observed (Figure 4d–e).

The NP nanostructures bear very little resemblance to the spherical supramolecule morphology, suggesting that at high NP loadings the self-assembly mechanism may be quite complex. At low NP loadings (3 vol %), the NP cluster morphology closely resembles the supramolecule morphology without NP loading; thus, in this case the supramolecule may serve as a structural scaffold to guide the NP assembly. In the case of parallel NP array morphology, the NPs may increase the volume fraction of the P4VP(PDP) microdomain such that it assembles into a cylindrical morphology with the axis of the cylinder directed parallel to the pore axis, such that the BCP chain stretching is azimuthally uniform. At a higher NP loading (6–9 vol %), the stacked rings and helical NP structures no longer correspond to the supramolecule structure. One possible explanation for this deviation is that the observed morphologies are simply the result of frustrated NP packing due to high NP loading and are independent of supramolecule morphology. However, control experiments using just blends of NP and P4VP(36.3 kDa)(PDP)$_1$ homopolymer-based supramolecules with 6 vol % and 9 vol % Au NP loadings show no ordered structures under cylindrical confinement (SI 5). Morphologies unique to unconfined BCPs, such as toroids and helices, have been observed in BCP systems as manifestations of the cylindrical morphology under 2-D confinement. These morphologies occur due to polymer chain frustration and symmetry breaking as the confining geometry approaches the natural BCP periodicity. Thus, it is possible that the nanostructures observed in the cylindrically confined supramolecular nanocomposites are also the result of additional NP loading increasing the P4VP(PDP) volume fraction of the supramolecule into the cylindrical morphology regime. The parallel to perpendicular transition in the morphology is favorable because the system has more freedom to relieve BCP chain stretching and accommodate any changes in the periodicity of the nanostructures along the pore axis.

All TEM images are representative of the specific nanocomposite. However, it is common to observe other morphologies in the same sample. The NP nanostructure distribution is counted from over 100 TEM images and plotted for each NP loading (Figure 5). As seen, there is a general trend of forming complex 3-D NP assembly as the NP loading increase. The system morphological degeneracy is evident. The morphological degeneracy between unconfined and cylindrically confined states has been theoretically predicted for both BCP and BCP/NP blends.[51−55] The degeneracy occurs when different states are similar in energy. Since the supramolecular system appears to self-adjust to mediate geometric frustration,

DOI: 10.1021/acs.nanolett.7b03131
Nano Lett. 2017, 17, 6847–6854

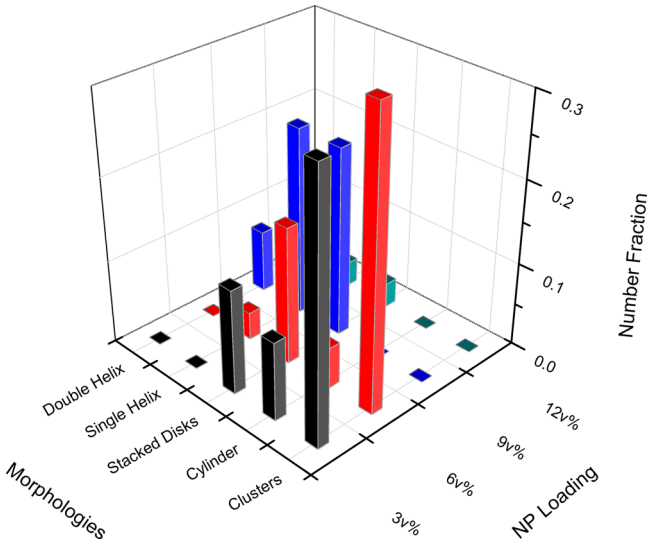

Figure 5. Frequency of nanostructures observed in PS-*b*-P4VP-$(PDP)_{1.7}$ supramolecule/Au NP nanocomposites under cylindrical confinement within AAO membrane pores is plotted below as a function of NP loading. The statistics are obtained from analysis of 100 TEM images.

it should have greater tendency to have system degeneracy due to rather flat energy landscape. Experimentally, the degeneracy may also be amplified due to the slight deviations in pore shape and diameter, which perturb the confinement conditions and overall entropic landscape of the nanocomposite system. Furthermore, the local NP loading also appears to be different when the nanowire morphology varies. It may be attributed to the NP diffusion into the nanowire as a result of increasing local PDP loading. The presence of NP also affects the local mobility and assembly kinetics. A high NP loading can lead to system jam and kinetically traps the system. This may explain the observed disordered assembly at a 12 vol % NP loading (SI 6).

Nevertheless, the experimental observations further indicate the complexities of supramolecular systems that challenge our basic understanding in multicomponent systems. The simple addition of the small PDP molecule, has many advantages such as ease of NP incorporation, modulation of polymer architecture, and potential route to release entropic conformational penalty. However, the presence of a small molecule that can be reversibly attached to a polymer side chain does lead to many changes in terms of intermolecular interactions between each component, entropic spring constant of polymer, volume fraction of each microdomain, and diffusion rate of each component. Although it is challenging to perform theoretical study that captures all the elements, computational investigation will provide great insights to delineate effects from many parameters and guidance to perform experiments to access novel assemblies.

Conclusion. In summary, we experimentally realized complex 3-D NP assemblies that have not been obtained before in the nanocomposite system, narrowing the gap between structural complexity between polymer/NP blends and the DNA approach. We show that, upon forming cylindrically confined nanowires of supramolecular nanocomposites, diverse NP assemblies inaccessible previously, such as stacked rings and single and double helical ribbons, can be obtained by varying the NP loading in a single supramolecule. Strong chiral plasmonic activity has been observed in the resultant helical NP ribbon at near-infrared region, beyond what was seen in helical single nanoparticle chains. Varying NP loading is more effective to obtain complex 3-D NP assemblies than that of supramolecule. At moderate NP loadings, the NP assemblies bear very little resemblance to the supramolecule morphology. The resultant NP assemblies appear to be governed by the most efficient way to pack NPs within a cylindrical nanowire. However, the periodicity is mainly governed by that of supramolecule. The supramolecular system adjusts small molecule distribution to mediate NP/polymer interaction and modulate NP assembly, opening opportunities to fabricate designed NP assemblies toward next generation metameterials and optoelectronic devices. Moreover, the energy landscape of supramolecular system differs from that of pure BCP, providing opportunities in adding complexity of system self-modulation with further in-depth investigation.

Experimental Section. *Materials.* P4VP and PS-*b*-P4VP block copolymers were purchased from Polymer Source, Inc. 3-Pentadecylphenol (PDP), hydrogen tetrachloroaurate (III) hydrate ($HAuCl_4 \cdot 3H_2O$), *tert*-butylamine-borane (TBAB, 97%), oleylamine (OA, 70% C18 content), 1,2,3,4-tetrahydronaphthalene (tetralin, 95%), and 1-dodecanethiol (DDT) are purchased from Sigma-Aldrich and used without further purification. AAO membranes were purchased from Synkera Technologies Inc.

Supramolecule Preparation. PS-*b*-P4VP was first dissolved in chloroform to form 1−2% (w/v) stock solution. The desired amount of PDP was dissolved in chloroform separately. The PS-*b*-P4VP solution was then added dropwise to the PDP solution, followed by stirring overnight.

Nanoparticle Synthesis. Au NPs were synthesized following a method published by Peng et al.[56] For a typical synthesis, 200 mg of $HAuCl_4 \cdot 3H_2O$ was dissolved in a mixture of 20 mL of oleylamine and 20 mL of tetralin solution and stirred for 30 min under N_2 gas at room temperature. Then, 86 mg of TBAB dissolved in 2 mL of oleylamine and 2 mL of tetralin was added to the solution to reduce the gold salt. The reaction was stirred for a further 1 h, and the NPs are purified by washing with acetone and chloroform. All NP size distributions were obtained using Igor Pro and ImageJ.

Nanowire Preparation. Supramolecule solution and Au NP solution are mixed together and drop-casted on top of an AAO membrane. The dried nanocomposite is then thermal annealed at 150 °C for 24 h under vacuum. The residual nanocomposite material on the membrane surface is subsequently removed, and the AAO template is dissolved to yield supramolecule/Au NP nanowires with cylindrically confined nanostructures.

SEM. Nanowire samples were deposited on a Si substrate and coated with 2 nm of gold in a Denton Vacuum thin film sputter station. SEM images are taken using a JEOL field emission SEM operating at 5.0 kV accelerating voltage and a working distance of 6.0 mm.

TEM. Nanotube samples were deposited on carbon-coated Cu grids and allowed to dry. Supramolecule nanowires were selectively stained with iodine to highlight the P4VP(PDP) microdomains as darker regions. The samples are imaged using a FEI Tecnai 12 TEM operating at 120 kV accelerating voltage or a JEOL 1200EX TEM operating at 80 kV.

TEM Tomography. TEM tomography was collected using an FEI Ultratwin Tecnai F20 operated at 200 kV and a Hummingbird Scientific high-tilt tomography holder. The tilt series were acquired from −70° to 70° with 1° tilt step increments and pixel resolution of 0.43 nm. Postprocessing

DOI: 10.1021/acs.nanolett.7b03131
Nano Lett. 2017, 17, 6847−6854

alignment and tomographic reconstruction of the tilt images were processed using the eTomo software package. IMOD and the Avizo 7.0 software packages were used for 3-D visualization.

Dark Field Scattering Microscopy. The CD signal of single Au NP helix was recorded using a home-built inverted optical microscope (Axiovert 200, Carl Zeiss MicroImaging Inc., Thornwood, NY) equipped with a dark-field objective (100×, NA = 0.9). The sample was prepared by drop-casting nanohelix on TEM grid. The white light from a halogen lamp passes through a polarizer followed by a quarter waveplate which converts linear polarization to circular polarization (see schematic in SI 3). By rotating the fast axis of the quarter wave-plate set to −45° and +45° with respect to the axis of the polarizer, left-handed and right-handed circular polarization was generated respectively and coupled into a dark-field reflector and objective to excite the structure. Then the CD spectrum was recorded by subtracting the spectrum for right-handed circular polarization from that taken with left-handed circular polarization and normalized to the intensity of light source. All data analysis was original without smoothing.

Method of CD Spectra Simulation. The CD responses of chiral plasmonic nanoparticle assemblies were simulated by using commercial software package CST Microwave Studio using finite integration technique (FIT) in frequency domain. The polymer index of 1.6 in which the nanoparticle are embedded was used as medium index, and the radius (25 nm) and pitch (50 nm) of helical NP ribbon (3 NPs across) were employed for simulation according to TEM image. The chiral structure was excited by left-handed and right-handed circular polarized plane waves, respectively. Then the CD signal was collected by normalizing the difference between scattering signal in far field of left (S_L)- and right (S_R)-handed excitation in frequency domain. The simulated spectrum (Figure 2a) shows a bisignate peak in the 700−1000 nm range which arises from the collective cross coupling of plasmonic dipole of Au NPs and phase lag along the propagation direction of the excitation light beam. Due to the phase lag along the propagation direction of the excitation light beam, a time-domain right-handed polarization rotating light will build "left-handed" polarization rotating light along this propagation direction in space. Therefore, Coulomb repulsion of the induced charges for a right-handed plasmonics NP chain under right-handed light excitation is higher than the case when it is excited by left-handed light. As a result, a right-handed plasmonic NP chain is expected to have resonance wavelength split with a lower energy (higher wavelength) resonance preference for left-handed light excitation, and vice versa.

■ ASSOCIATED CONTENT

Supporting Information

The Supporting Information is available free of charge on the ACS Publications website at DOI: 10.1021/acs.nanolett.7b03131.

TEM of nanoparticles and nanowire composites and method of CD spectra simulation and dark field scattering microscopy (PDF)

Video of 3-D TEM tomography reconstruction of nanowires with single helix morphologies (MPG)

Video of 3-D TEM tomography reconstruction of nanowires with stacked ring morphologies (MPG)

■ AUTHOR INFORMATION

Corresponding Author

*E-mail: tingxu@berkeley.edu.

ORCID

Miquel Salmeron: 0000-0002-2887-8128

Ting Xu: 0000-0002-2831-2095

Funding

This work was funded by the U.S. Department of Energy, Office of Science, Office of Basic Energy Sciences, Materials Sciences and Engineering Division under contract no. DE-AC02-05-CH11231 (Organic−Inorganic Nanocomposites KC3104) (P.B., W.B., J.K., K. T., M.S. and T.X.). Work (TEM tomography) at the Molecular Foundry was supported by the Office of Science, Office of Basic Energy Sciences, of the U.S. Department of Energy under contract no. DE-AC02-05CH11231. S. Y., W. B., and X. Z. acknowledge support from the Director, Office of Science, Office of Basic Energy Sciences, Materials Sciences, and Engineering Division of the US Department of Energy within the Metamaterials Program (KC12XZ).

Notes

The authors declare no competing financial interest.

■ ACKNOWLEDGMENTS

We thank Dr. Peter Ercius and Dr. Chengyu Song at the National Center for Electron Microscopy for their helpful advice and support for TEM tomography studies.

■ REFERENCES

(1) Alivisatos, A. P.; Johnsson, K. P.; Peng, X. G.; Wilson, T. E.; Loweth, C. J.; Bruchez, M. P.; Schultz, P. G. *Nature* **1996**, *382*, 609−611.

(2) Chen, C.-L.; Rosi, N. L. *J. Am. Chem. Soc.* **2010**, *132*, 6902−6903.

(3) Kuzyk, A.; Schreiber, R.; Fan, Z.; Pardatscher, G.; Roller, E.-M.; Hoegele, A.; Simmel, F. C.; Govorov, A. O.; Liedl, T. *Nature* **2012**, *483*, 311−314.

(4) Mastroianni, A. J.; Claridge, S. A.; Alivisatos, A. P. *J. Am. Chem. Soc.* **2009**, *131*, 8455−8459.

(5) Mirkin, C. A.; Letsinger, R. L.; Mucic, R. C.; Storhoff, J. J. *Nature* **1996**, *382*, 607−609.

(6) Nie, Z.; Petukhova, A.; Kumacheva, E. *Nat. Nanotechnol.* **2010**, *5*, 15−25.

(7) Sharma, J.; Chhabra, R.; Cheng, A.; Brownell, J.; Liu, Y.; Yan, H. *Science* **2009**, *323*, 112−116.

(8) Talapin, D. V.; Murray, C. B. *Science* **2005**, *310*, 86−89.

(9) Tan, S. J.; Campolongo, M. J.; Luo, D.; Cheng, W. *Nat. Nanotechnol.* **2011**, *6*, 268−276.

(10) Lan, X.; Wang, Q. *Adv. Mater.* **2016**, *28*, 10499−10507.

(11) Warren, S. C.; DiSalvo, F. J.; Wiesner, U. *Nat. Mater.* **2007**, *6*, 156−161.

(12) Pickett, G. T.; Gross, M.; Okuyama, H. *Phys. Rev. Lett.* **2000**, *85*, 3652−3655.

(13) Yin, Y. D.; Xia, Y. N. *J. Am. Chem. Soc.* **2003**, *125*, 2048−2049.

(14) Cui, Y.; Björk, M. T.; Liddle, J. A.; Sönnichsen, C.; Boussert, B.; Alivisatos, A. P. *Nano Lett.* **2004**, *4*, 1093−1098.

(15) Bockstaller, M. R.; Lapetnikov, Y.; Margel, S.; Thomas, E. L. *J. Am. Chem. Soc.* **2003**, *125*, 5276−5277.

(16) Kao, J.; Thorkelsson, K.; Bai, P.; Rancatore, B. J.; Xu, T. *Chem. Soc. Rev.* **2013**, *42*, 2654−2678.

(17) Dobriyal, P.; Xiang, H.; Kazuyuki, M.; Chen, J.-T.; Jinnai, H.; Russell, T. P. *Macromolecules* **2009**, *42*, 9082−9088.

(18) Xiang, H.; Shin, K.; Kim, T.; Moon, S. I.; McCarthy, T. J.; Russell, T. P. *Macromolecules* **2004**, *37*, 5660−5664.

(19) Rahikkala, A.; Soininen, A. J.; Ruokolainen, J.; Mezzenga, R.; Raula, J.; Kauppinen, E. I. *Soft Matter* **2013**, *9*, 1492−1499.

DOI: 10.1021/acs.nanolett.7b03131
Nano Lett. 2017, 17, 6847−6854

(20) Chiu, J. J.; Kim, B. J.; Yi, G.-R.; Bang, J.; Kramer, E. J.; Pine, D. J. *Macromolecules* **2007**, *40*, 3361−3365.
(21) Thompson, R. B.; Ginzburg, V. V.; Matsen, M. W.; Balazs, A. C. *Science* **2001**, *292*, 2469−2472.
(22) Kao, J.; Bai, P.; Chuang, V. P.; Jiang, Z.; Ercius, P.; Xu, T. *Nano Lett.* **2012**, *12*, 2610−2618.
(23) Arora, H.; Du, P.; Tan, K. W.; Hyun, J. K.; Grazul, J.; Xin, H. L.; Muller, D. A.; Thompson, M. O.; Wiesner, U. *Science* **2010**, *330*, 214−219.
(24) Du, P.; Li, M.; Douki, K.; Li, X.; Garcia, C. B. W.; Jain, A.; Smilgies, D. M.; Fetters, L. J.; Gruner, S. M.; Wiesner, U.; Ober, C. K. *Adv. Mater.* **2004**, *16*, 953−957.
(25) Simon, P. F. W.; Ulrich, R.; Spiess, H. W.; Wiesner, U. *Chem. Mater.* **2001**, *13*, 3464−3486.
(26) Templin, M.; Franck, A.; Du Chesne, A.; Leist, H.; Zhang, Y.; Ulrich, R.; Schädler, V.; Wiesner, U. *Science* **1997**, *278*, 1795−1798.
(27) Ruokolainen, J.; Saariaho, M.; Ikkala, O.; ten Brinke, G.; Thomas, E. L.; Torkkeli, M.; Serimaa, R. *Macromolecules* **1999**, *32*, 1152−1158.
(28) Zhao, Y.; Thorkelsson, K.; Mastroianni, A. J.; Schilling, T.; Luther, J. M.; Rancatore, B. J.; Matsunaga, K.; Jinnai, H.; Wu, Y.; Poulsen, D.; Frechet, J. M. J.; Alivisatos, A. P.; Xu, T. *Nat. Mater.* **2009**, *8*, 979−985.
(29) Shen, X.; Song, C.; Wang, J.; Shi, D.; Wang, Z.; Liu, N.; Ding, B. *J. Am. Chem. Soc.* **2012**, *134*, 146−149.
(30) Chen, C.-L.; Zhang, P.; Rosi, N. L. *J. Am. Chem. Soc.* **2008**, *130*, 13555−13557.
(31) Song, C.; Blaber, M. G.; Zhao, G.; Zhang, P.; Fry, H. C.; Schatz, G. C.; Rosi, N. L. *Nano Lett.* **2013**, *13*, 3256−3261.
(32) Jung, S. H.; Jeon, J.; Kim, H.; Jaworski, J.; Jung, J. H. *J. Am. Chem. Soc.* **2014**, *136*, 6446−6452.
(33) Arnold, M. D.; Blaber, M. G.; Ford, M. J.; Harris, N. *Opt. Express* **2010**, *18*, 7528−7542.
(34) Schreiber, R.; Luong, N.; Fan, Z.; Kuzyk, A.; Nickels, P. C.; Zhang, T.; Smith, D. M.; Yurke, B.; Kuang, W.; Govorov, A. O.; Liedl, T. *Nat. Commun.* **2013**, *4*, 2948.
(35) Hentschel, M.; Wu, L.; Schaferling, M.; Bai, P.; Li, E. P.; Giessen, H. *ACS Nano* **2012**, *6*, 10355−10365.
(36) Kuhn, W. *Trans. Faraday Soc.* **1930**, *26*, 293−307.
(37) Esposito, M.; Tasco, V.; Cuscuna, M.; Todisco, F.; Benedetti, A.; Tarantini, I.; De Giorgi, M.; Sanvitto, D.; Passaseo, A. *ACS Photonics* **2015**, *2*, 105−114.
(38) Bustamante, C.; Tinoco, I.; Maestre, M. F. *Proc. Natl. Acad. Sci. U. S. A.* **1983**, *80*, 3568−3572.
(39) Fan, Z.; Govorov, A. O. *Nano Lett.* **2010**, *10*, 2580−2587.
(40) Peer, N.; Dujovne, I.; Yochelis, S.; Paltiel, Y. *ACS Photonics* **2015**, *2*, 1476−1481.
(41) Lu, X. X.; Wu, J.; Zhu, Q. N.; Zhao, J. W.; Wang, Q. B.; Zhan, L.; Ni, W. H. *Nanoscale* **2014**, *6*, 14244−14253.
(42) Barron, L. D. *Molecular light scattering and optical activity*. Cambridge University Press, 2004.
(43) Kuzyk, A.; Schreiber, R.; Fan, Z. Y.; Pardatscher, G.; Roller, E. M.; Hogele, A.; Simmel, F. C.; Govorov, A. O.; Liedl, T. *Nature* **2012**, *483*, 311−314.
(44) Ma, W.; Kuang, H.; Xu, L. G.; Ding, L.; Xu, C. L.; Wang, L. B.; Kotov, N. A. *Nat. Commun.* **2013**, *4*, 8.
(45) Hendry, E.; Carpy, T.; Johnston, J.; Popland, M.; Mikhaylovskiy, R. V.; Lapthorn, A. J.; Kelly, S. M.; Barron, L. D.; Gadegaard, N.; Kadodwala, M. *Nat. Nanotechnol.* **2010**, *5*, 783−787.
(46) Stephens, P. J.; Devlin, F. J.; Pan, J.-J. *Chirality* **2008**, *20*, 643−663.
(47) Pendry, J. B. *Science* **2004**, *306*, 1353−1355.
(48) Shi, A.-C.; Li, B. *Soft Matter* **2013**, *9*, 1398−1413.
(49) Valkama, S.; Ruotsalainen, T.; Nykänen, A.; Laiho, A.; Kosonen, H.; ten Brinke, G.; Ikkala, O.; Ruokolainen, J. *Macromolecules* **2006**, *39*, 9327−9336.
(50) Kao, J.; Tingsanchali, J.; Xu, T. *Macromolecules* **2011**, *44*, 4392−4400.
(51) Sevink, G. J. A.; Zvelindovsky, A. V.; Fraaije, J.; Huinink, H. P. *J. Chem. Phys.* **2001**, *115*, 8226−8230.
(52) Li, W.; Wickham, R. A.; Garbary, R. A. *Macromolecules* **2006**, *39*, 806−811.
(53) Yu, B.; Sun, P.; Chen, T.; Jin, Q.; Ding, D.; Li, B.; Shi, A.-C. *Phys. Rev. Lett.* **2006**, *96*, 138306.
(54) Zhu, Y.; Jiang, W. *Macromolecules* **2007**, *40*, 2872−2881.
(55) Park, J. H.; Kalra, V.; Joo, Y. L. *Soft Matter* **2012**, *8*, 1845−1857.
(56) Peng, S.; Lee, Y.; Wang, C.; Yin, H.; Dai, S.; Sun, S. *Nano Res.* **2008**, *1*, 229−234.

DOI: 10.1021/acs.nanolett.7b03131
Nano Lett. 2017, 17, 6847−6854